Radiotherapy and Oncology 137 (2019) 32–37

Contents lists available at ScienceDirect

Radiotherapy and Oncology

journal homepage: www.thegreenjournal.com

Original Article

MRI-based tumour control probability in skull-base chordomas treated with carbon-ion therapy

Giulia Buizza [a,*], Silvia Molinelli [b], Emma D'Ippolito [b], Giulia Fontana [b], Andrea Pella [b], Francesca Valvo [b], Lorenzo Preda [b,c], Roberto Orecchia [b], Guido Baroni [a,b], Chiara Paganelli [a]

[a] Department of Electronics, Information and Bioengineering, Politecnico di Milano; [b] National Center of Oncological Hadrontherapy (CNAO), Pavia; and [c] Department of Clinical, Surgical, Diagnostic and Pediatric Sciences, University of Pavia, Italy

ARTICLE INFO

Article history:
Received 14 January 2019
Received in revised form 30 March 2019
Accepted 18 April 2019
Available online 30 April 2019

Keywords:
Diffusion Magnetic Resonance Imaging
Heavy ion radiotherapy
Chordoma
Skull base

ABSTRACT

Purpose: To derive personalized tumour control probability (TCP) models, using diffusion-weighted (DW-) MRI for defining initial tumour cellular density in skull-base chordoma patients undergoing carbon-ion radiotherapy (CIRT).

Materials and methods: 67 patients affected by skull-base chordoma were enrolled for a standardized CIRT treatment (70.4 Gy (RBE) prescription dose). Local control information was clinically assessed. For 20 of them, apparent diffusion coefficient (ADC) maps were computed from DW-MRI and then converted into cellular density. Radiosensitivity parameters (α, β) were estimated from the available data through an optimization procedure, taking advantage of a relationship observed between local control and the dose received by at least the 98% of the gross tumour volume. These parameters were fed into two poissonian TCP models, based on the LQ model, being the first (TCP_{LIT}) computed from literature parameters and the second (TCP_{ADC}) enriched by a personalized initial cellular density derived from ADC maps.

Results: The inclusion of the cellular density derived from ADC into TCP_{ADC} yielded slightly higher dose values at which TCP = 0.5 (D_{50} = 38.91 Gy (RBE)) with respect to TCP_{LIT} (D_{50}34.16 Gy (RBE)). This suggested a more conservative approach, even if the prognostic power of TCP_{ADC} and TCP_{LIT}, tested with respect to local control, was equivalent in terms of sensitivity (0.867) and specificity (0.600).

Conclusions: Both TCP_{ADC} and TCP_{LIT} exhibited good agreement with a clinically validated information of local control, the former providing more conservative predictions.

Particle therapy makes use of protons and heavier ions to improve geometrical and biological efficacy in terms of dose distribution, with respect to photons, thus enabling tumour dose escalation whilst sparing the surrounding healthy tissues. Although protons have a biological effectiveness comparable to photons, this is higher for heavy ions [1]. In particular, carbon-ion radiotherapy (CIRT) has been found to perform well with radioresistant tumours close to organs at risk [2], such as chordoma tumours [3].

Skull-base chordoma is an aggressive, locally invasive and poorly prognosed cancer. Its management is still nowadays critical: the slow growth coupled with strong aggressiveness, frequent recurrence, invasiveness towards bone and neural structures, lower the effectiveness of surgical resection and radiation treatments [4]. Particle therapy is currently considered as the ideal modality for skull-base chordomas [5]. In particular, post-surgical CIRT was proved to be effective [6–8] and allowed to escalate the dose to the tumour up to 70–80 Gy (RBE). However, the rarity of skull-base chordomas did not favour their molecular and radiological characterization until recent years [9,10] and the relevance of different prognostic factors remains uncertain [11]. Therefore, a deeper understanding of the relationship between the effects of CIRT and the observed tumour control could meaningfully complement the ongoing characterization of skull-base chordomas.

Well-established mathematical models defining tumour control probability (TCP) describe the probability of eradicating the tumour, which clinically corresponds to achieve local control (LC). Along the years, they have been theoretically framed [12–14] to enhance the contribution of the planned dose, modulated by radiobiological parameters, to LC prediction. However, little information related to the underlying in-vivo biology, characterized by an extremely high variability that could hinder the robustness of such models, was included. Radiobiological parameters are conventionally estimated from in-vitro cell-plating experiments, that cannot fully describe intra- and inter-patient variabilities [15], or from dose escalation trials [16]. These studies are not always feasible, the statistics is poor and, most importantly, they cannot account for patient heterogeneities. The biological

* Corresponding author at: piazza Leonardo da Vinci 32, 20133 Milano, Italy.
E-mail address: giulia.buizza@polimi.it (G. Buizza).

https://doi.org/10.1016/j.radonc.2019.04.018
0167-8140/

variabilities amongst and within patients, however, do influence the therapeutic outcome of radiotherapy and efforts are needed to make the most of related quantitative data, in order better tailor treatment planning strategies, especially in CIRT [17].

Medical imaging can bring patient-specific information into these models, describing intra-patient heterogeneity at the voxel scale. Amongst imaging techniques, Magnetic Resonance Imaging (MRI) has gained a particular relevance in the radiation oncology workflow over the last decade [18,19] and various MR techniques can provide 3D spatial maps of anatomical and functional information. Diffusion-weighted (DW-) MRI is a well-established method to characterize oncological lesions in terms of cellular density, proliferation power and cellular permeability, by means of apparent diffusion coefficient (ADC) maps [20,21]. The inclusion of this information at the cellular level in TCP models is believed to substantially increase the accuracy with which tumour control can be predicted. In a recent study [22], ADC maps were computed from DW-MRI before X-ray radiotherapy and from them cancerous cellular density was estimated. This study showed that the use of MRI-driven cellular density can enhance differences in TCP amongst patients, suggesting a better representation of patient-specific characteristics. In this context, the higher influence of biological factors in the therapeutic effectiveness of CIRT doses, has recently put forward the need for studies in which models are built upon biological information derived from MRI to improve tumour characterization and clinical outcome [23–25].

The aim of this study was to evaluate the use of DW-MRI for modelling TCP in patients affected by skull-base chordomas and enrolled for a well-defined CIRT protocol, paving the way towards personalized and optimized treatments. Heterogeneous cellular density, from ADC maps, and dose distributions were evaluated to build an MRI-based TCP, which was compared to a model fed with conventional parameters from the literature and assessed with respect to the clinical LC observed during patients' follow-up.

Materials and methods

Data

From 2013 to 2018, 67 patients affected by skull-base chordoma were treated with CIRT at 70.4 Gy (RBE) prescribed dose (4.4 Gy (RBE), 16 fractions), at Anonymous Institution XXX, after partial surgical resection. Written informed consent was obtained before treatment started. After a median follow-up of 31 months (range: 6–66 months) LC was 76%. A positive LC (LC = 1) was defined as a progression-free evaluation at follow-up, whereas a negative one (LC = 0) indicated recurrence or disease progression in the target volume. If the LC was influenced by factors unrelated to the therapy, patients were excluded from the study. All enrolled patients underwent CT scans for contouring and treatment planning (TPS Syngo RT Planning VC13, Siemens Medical Systems, Erlangen, Germany), as well as anatomical MR scans to improve the contouring phase. From this dataset, 20 patients were retrospectively selected to define a homogeneous dataset for the specific set of b-values at which DW-MRI were acquired. For these patients, DW-MRI were acquired on a 3T clinical scanner (Magnetom Verio, Siemens Medical Systems, Erlangen, Germany) with an echo-planar (EPI) sequence at 3b-values (50, 400 and 1000 s/mm^2) as the average diffusion value along three orthogonal axes (TR = 4600–13300 s, TE = 72–95 s, flip angle = 90, resolution = 1.30–1.97 mm, slice spacing = 5.2–6 mm, GRAPPA accelerator factor = 2, EPI factor = 132). ADC maps were computed on-scanner using all b-values. For the selected patients, quantities summarizing dose distributions in the gross tumour volume (GTV), GTV volume, follow-up time and LC are given in Table 1.

MRI-based cellularity estimation

The estimation of the relationship between ADC and cellular density (ρ_0) was based on a histological study from the literature [26], in which the minimum ADC in the tumour normalized by the minimum ADC in normally appearing white matter was related to the overall number of cells for different malignant lesions. The chordoma included in that study was characterized by 276 cells/FOV (FOV = 660 * 495 μm^2).

In this study, the ADC was normalized by the 5th percentile of the ADC distribution in the normally appearing white matter, as more robust to noise than the minimum value. By assuming that the histological plate was as thick as a cell and that the median diameter of a cell was 11 μm [27], it was possible to estimate the number of cells in a volumetric FOV and subsequently the ρ_0 in the voxel. Different ADC-ρ_0 relationships were also evaluated, as reported in the Supplementary material S1. Then, ADC maps were rigidly registered to CT scans to establish a voxel-wise spatial correspondence between ρ_0, dose and GTV contours.

Tumour control probability (TCP)

The linear-quadratic (LQ) model [28] for cell survival and the Poisson model for cell killing were employed to estimate the survival fraction (*SF*) and the TCP (Fig. 1), respectively. The *SF* after n fractions of dose d was defined as $SF = \exp[-\alpha \cdot n \cdot d \cdot (1 + \beta/\alpha \cdot d)]$, where α and β are the linear and the quadratic radiosensitivity coefficients. By applying the Poisson model of cell killing, the TCP was defined as in Eq. (1)

$$TCP = \prod_{b=1}^{B} - N_0 \cdot exp\left[-\alpha \cdot n \cdot d_b\left(1 + \tfrac{\beta}{\alpha} \cdot d_b\right)\right], \quad (1)$$

where $N_0 = \rho_0 \cdot V$ is the initial number of cells, given by ρ_0 and the volume V, and d_b is the dose delivered to the bth voxel according to the treatment plan. The TCP of the whole patients' population was obtained by fitting TCP values from all GTVs to a sigmoidal curve (Eq. (2)) using the Levenberg–Marquardt algorithm (a and b fitting parameters).

$$TCP = \tfrac{1}{1+e^{a+b\,d}} \quad (2)$$

Inter-patient differences in radiosensitivity were taken into account by describing α with a log-normal distribution, as it is a non-negative parameter with high variability [29]. An average value over the whole population (α_{POP}) was estimated by setting the TCP of the whole population (TCP_{POP}) to 0.76, ρ_0 equal to 10^7 cm^{-3} [13,30] and d_b was the dose received by at least 98% of the GTV ($D_{98\%}$) in Eq. (1). $D_{98\%}$ was chosen as d_b, instead of the most commonly used $D_{50\%}$, as an indication of the minimum dose delivered to the target [31] that highly affects poissonian TCP models. The impact of cold spots on the TCP and the similarity of $D_{50\%}$ across patients, together with a good observed correlation (Fig. 2), supported such choice.

The mode of the log-normal distribution was set to be the estimated average α_{POP} and the standard deviation to be 0.15, as defined in [22]. For each patient, 10 values of α were randomly sampled from the log-normal distribution and the TCP values for a single patient were defined by the average of the 10 values obtained for different α, along different dose bins [32] (dose binning with fixed counts equal to 2% of the GTV volume). Weights for these 10 TCP values were defined as the probability of a certain α to occur and normalized to sum up to unity for a single patient [29].

Two radiosensitivity parameters configurations were tested for Eq. (1): either β was set to 0, to reproduce the mainly linear response in CIRT [33], or according to $\alpha/\beta = 2$ Gy^{-1} (3).

Different approaches were considered when feeding ρ_0 into the TCP. Specifically, two TCP models were built:

Table 1
Patients characteristics in terms of dose, gross tumour volume (GTV), time between the end of the treatment and follow-up, local control (LC). $D_{98\%}$ = dose received by at least 98% of the GTV; $D_{95\%}$=dose received by at least 95% of the GTV; IQR = interquartile range.

Patient	$D_{50\%}$/Gy (RBE)	$D_{98\%}$/Gy (RBE)	$D_{95\%}$/Gy (RBE)	GTV volume/ml	Follow-up time/months	LC
1	70,70	56,79	63,05	20,01	55,14	1
2	71,71	62,05	66,88	11,03	50,25	1
3	74,92	34,52	49,37	60,13	14,64	0
4	71,18	68,25	69,67	12,87	43,93	1
5	71,68	40,37	53,17	127,00	5,71	0
6	71,14	68,25	68,63	1,14	45,21	1
7	70,88	46,69	55,96	18,84	39,61	0
8	71,79	54,90	60,54	17,04	50,32	1
9	72,75	57,98	62,35	5,45	46,43	1
10	70,08	40,61	45,90	4,08	53,11	1
11	71,30	59,52	63,29	5,22	51,11	1
12	73,71	58,58	65,24	2,65	49,00	1
13	69,76	47,59	53,56	3,22	46,57	1
14	71,15	40,75	52,70	3,97	53,07	0
15	71,32	53,83	60,02	15,02	49,00	1
16	71,36	45,15	52,01	2,11	32,14	0
17	71,38	30,53	37,31	50,14	32,46	1
18	71,00	65,11	68,41	23,69	41,54	0
19	72,54	65,36	70,39	15,08	21,82	1
20	71,46	42,68	49,44	33,05	30,00	0
Median	71,34	54,37	60,28	13,95	45,82	65%
IQR	0,63	17,96	13,12	16,88	17,88	–

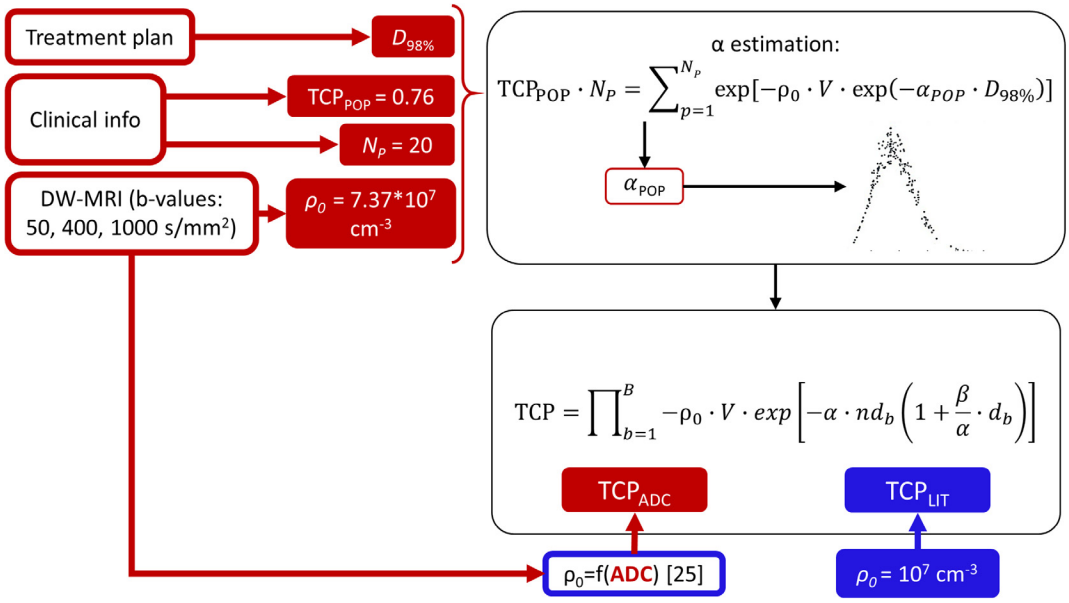

Fig. 1. Overview of parameters and methods applied to estimate TCP_{ADC} and TCP_{LIT}. Patient-specific and literature information is displayed in red and blue, respectively.

(i) an ADC-based TCP (TCP_{ADC}), in which ρ_0 was computed from ADC maps. In this case, either the voxel-wise ρ_0 or the median ρ_0 computed from the GTV of all patients was fed into the TCP model;
(ii) a literature-based TCP (TCP_{LIT}), in which ρ_0 was fixed to 10^7 cm^{-3} [13,30].

A thorough description of the methodology is reported in S2. In the Results section, all findings are reported for $\beta = 0$ and, for TCP_{ADC}, median ρ_0. Additional results for other settings of radiosensitivity parameters and cellular density estimation are reported in Supplementary material S3.

Model evaluation

The analysis of the TCP_{ADC} and TCP_{LIT} models consisted in verifying the agreement in the relationship between LC and $D_{98\%}$ and evaluating the quality of the fit to clinical data by means of the R^2 and the confidence intervals (CI, 95% confidence) of a and b (Eq. (2)), respectively. Finally, receiver operating characteristic (ROC) curves were built to compare the TCP models with the LC for each patient. Such comparison was performed in terms of sensitivity, specificity and area under the curve (AUC, with pointwise CI at 95% confidence).

Results

The relationship between LC or TCP and $D_{98\%}$ was observed and confirmed by the good quality of the fit, being the R^2 0.844 for LC, 0.978 for TCP_{ADC} and 0.975 for TCP_{LIT} (Fig. 2).

This dependency and the spread of $D_{98\%}$ values across patients (Table 1) were exploited to estimate α_{POP} in case of patients with the same prescribed dose (70.4 Gy (RBE)) and, consequently, simi-

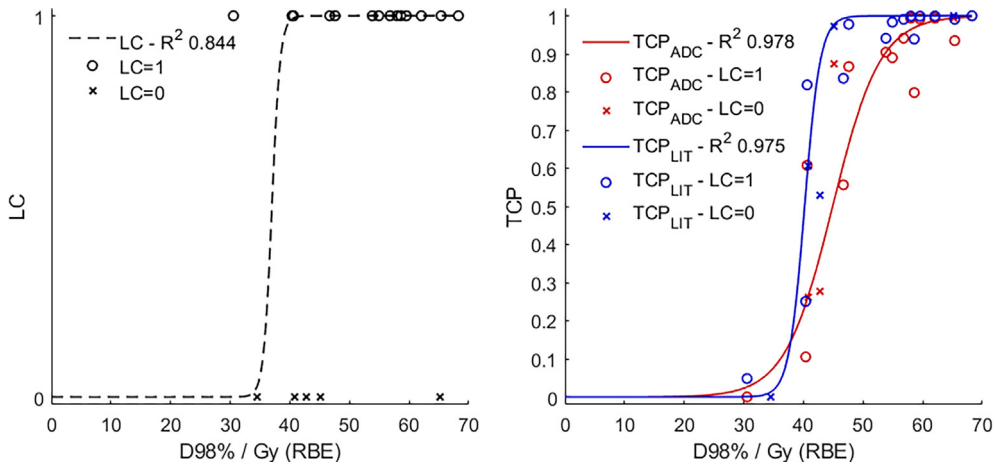

Fig. 2. On the left, local control (LC) fitted as a function of $D_{98\%}$ for patients with positive (circles) or negative (crosses) LC. On the right, TCP_{ADC} and TCP_{LIT} fits and data points as functions of $D_{98\%}$. R^2 for each fit is reported in the legend.

lar $D_{50\%}$. The resulting α_{POP} when $\beta = 0$ was found to be 0.470 Gy^{-1} and used to define the mode of the α log-normal distribution. TCPs agreed for different configurations of radiosensitivity parameters, as reported in Table S1 of the Supplementary material.

As far as cellular density is concerned, a linear relationship between ADC and ρ_0 was estimated, as shown in Fig. 3c. Fig. 3a and b show also two representative cases for LC = 1 and LC = 0. Overall, ρ_0 ranged from 7.338 to 7.408 $\cdot 10^7$ cm^{-3}, with ADC ranging from 508 to 1444 $\cdot 10^{-6}$ mm^2/s; the median ρ_0 was 7.365 $\cdot 10^7$ cm^{-3}, which corresponded to a median ADC of 1177 $\cdot 10^{-6}$ mm^2/s.

Radiosensitivity parameters and cellular densities were used to compute TCP values for each patient and the TCP curves for the whole population were fit to these datapoints. Generally, a lower prediction of local control resulted for TCP_{ADC} with respect to TCP_{LIT} (Fig. 4a). When feeding the TCP model with an ADC-dependent ρ_0, D_{50} (i.e. the dose at which TCP = 0.5) was 38.87 Gy (RBE), whereas it was 34.17 Gy (RBE) when using a literature-derived cellular density ($\rho_0 = 10^7$ cm^{-3}). Similarly, γ_{50} (i.e. the slope of the TCP curve at D_{50}) was lower for TCP_{ADC} (0.142 Gy $(RBE)^{-1}$) with respect to TCP_{LIT} (0.215 Gy $(RBE)^{-1}$). The parameters of the fitted sigmoidal function (Eq. (2)) were $a = 22.034$ ($CI_{95\%}$ = [21.917 22.150]) and $b = -0.567$ Gy $(RBE)^{-1}$ ($CI_{95\%}$ = [−0.570–0.564]) for TCP_{ADC} and $a = 29.424$ ($CI_{95\%}$ = [26.397 32.450]) and $b = -0.861$ Gy $(RBE)^{-1}$ ($CI_{95\%}$ = [−0.950–0.772]) for TCP_{LIT}.

The predictive performance of TCP models was assessed through ROC curves (Fig. 4b), built against the clinically provided LC. Sensitivity and specificity at the optimal point were 0.867 and 0.600 for both TCP_{ADC} and TCP_{LIT}. As well, the same AUC and comparable confidence intervals was observed (0.720, $CI_{95\%}$ = [0.333 0.953] for TCP_{ADC} vs. 0.720, $CI_{95\%}$ = [0.344 0.947] for TCP_{LIT}).

Discussion

In this study, the personalization of a dose–response TCP model fed by quantitative DW-MRI was evaluated for skull-base chordoma patients treated with CIRT. Aiming at better addressing inter- and intra-patient variabilities, cellular density was derived from ADC maps and included in a poissonian TCP model to better comply with patient-specific in-vivo characteristics.

Compared to a TCP model based on parameters from the literature, the model based on DW-MRI information showed a D_{50} higher by 13% and a γ_{50} lower by 40%, which agrees with the use of a seven-times higher ρ_0. Additionally, the $CI_{95\%}$ of the estimated

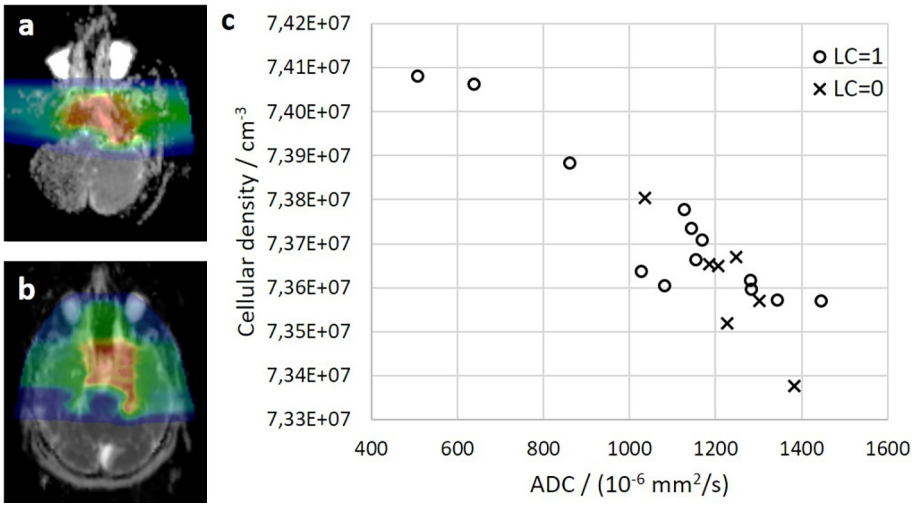

Fig. 3. An axial view of the dose distribution superimposed to an ADC map is shown for patients with either (a) a positive (median values: ADC = 638 * 10^{-6} mm^2/s, ρ_0 = 7.41 * 10^7 cm^{-3}) or (b) a negative local control (median values: ADC = 1248 * 10^{-6} mm^2/s, ρ_0 = 7.37 * 10^7 cm^{-3}). The relationship between the median values of ADC and cellularity in the GTV is shown in (c) for the 20 patients.

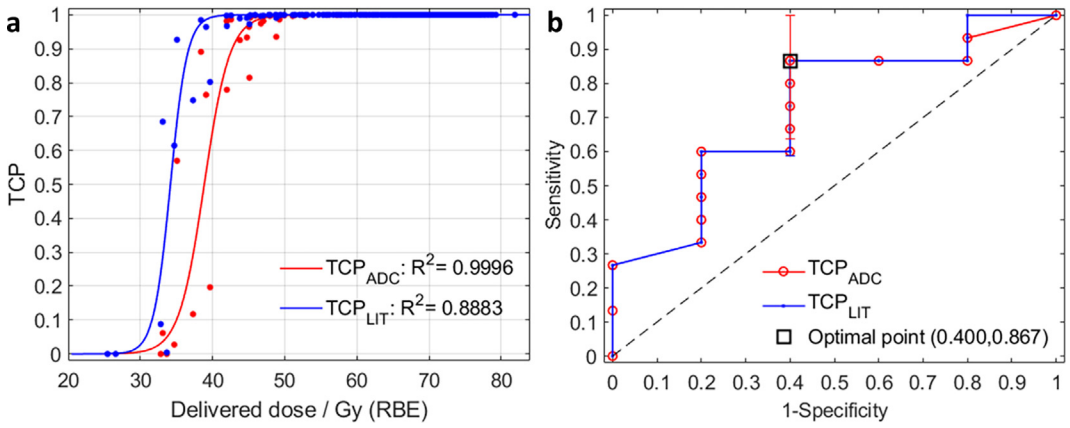

Fig. 4. On the left (a), TCP_{ADC} (D_{50} = 38.87 Gy (RBE), γ_{50} = 0.142 Gy (RBE)$^{-1}$) and TCP_{LIT} (D_{50} = 34.17 Gy (RBE), γ_{50} = 0.215 Gy (RBE)$^{-1}$) fits, R^2 and data points are shown as functions of the median value of the dose bin in the GTV. On the right (b), ROC curves for TCP_{ADC} (AUC = 0.707) and TCP_{LIT} (AUC = 0.720) are reported and the common optimal point (specificity = 0.600, sensitivity = 0.867) is highlighted in black.

a and b (fitting parameters in Eq. (2)) do not overlap and broader $CI_{95\%}$ are found for TCP_{LIT} with respect to TCP_{ADC}. This suggests a relevant difference between TCP_{ADC} and TCP_{LIT} fittings as well as a higher reliability of TCP_{ADC}.

In terms of comparison to the clinical outcome (LC), the AUC, sensitivity and specificity from ROC curves, of TCP_{ADC} and TCP_{LIT} were equivalent (Fig. 4b). Such similarity could be due to the fact that continuous (TCP) and binary (LC) variables were compared. Instead, a higher granularity of the clinical response (e.g. differentiating partial from complete response) and longer follow-up times could improve the adherence of the TCP models to clinical data. It should be noticed that the LC for the selected patients was lower (65%) than the overall cohort (76%), thus a thorough analysis would be required if the derived TCP was to be extended to the whole patient population.

As skull-base chordomas are almost surrounded by sensitive organs at risk (e.g. the brainstem), the dose constraints on such structures may generate low $D_{98\%}$ (34). The TCP formulation requires the treatment to eradicate all cancerous cells to achieve tumour control and the LQ-modelled cell survival fraction strongly depends on the planned dose. Consequently, even if low doses affect both TCP models, TCP_{ADC} seems to be more conservative than TCP_{LIT} with respect to the observed LC (Fig. 2), thus providing a more precautionary model when dealing with low $D_{98\%}$. This is expected to be beneficial in CIRT for evaluating of local dose effects [34] as well defining personalized treatments [17]. Nevertheless, for a comprehensive plan evaluation, future analyses should also complement the current analysis in terms of normal tissue complication probability models for critical healthy structures.

As for radiosensitivity parameters (α,β), these are typically computed by in-vitro studies or by fitting clinical data of patients' cohorts treated with different prescribed doses [16]. In this study, such data were not available, thus forcing an estimation of α from an observed relationship between $D_{98\%}$ and LC. The estimated α_{POP} was reasonable (α_{POP} = 0.47 Gy^{-1}) and comparable to values obtained from in-vitro experiments [33] on various brain tumours treated with CIRT (range: 0.04–2.16 Gy^{-1}). It was also found to be independent from the ρ_0 given as input, but it varied depending on the amount of repair (β) hypothesized in the TCP model (α_{POP} = 0.26 Gy^{-1} for $\beta \neq 0$, S2). The applicability of this method is limited by the lack of a comparison to traditional approaches that could be carried out for clinical cases in which dose-escalation studies are available. However, a robust estimation of variabilities is found to be challenging even in conventional radiotherapy [35] where more patient data exist. In the current study, the variability of the radiosensitivity parameters was modelled with a sampling approach [29], using a log-normal distribution to retain the biological meaning of the parameter ($\alpha > 0$, high variability) and a reasonable number of samples (n = 10) with respect to the number of patients (n = 20). If robust estimates of α and β variances were available for the specific patient group and treatment type under investigation, such variabilities could be directly embedded in the mathematical formulation of the TCP [22].

The main limitation of this study lies in the uncertainties related to the scale of the analysis (mm vs. μm) that inherently affect the relationship between ADC and the cellular density ρ_0 (Supplementary material S1). However, this is the parameter of the TCP model that can be non-invasively obtained for each patient. To the best of our knowledge, only one study reported the relationship between ρ_0 and ADC (b-values = 0,1000 s/mm^2) for one single patient affected by chordoma [26], because of the generally poor characterization of this tumour [36]. Such ADC was obtained with a different set of b-values and the reported single-point relationship does not allow the estimation of a linear relationship. Yet, the values of ρ_0 obtained in the current study agree with the literature [26]. Further studies involving more skull-base chordomas patients are needed to propose a more robust relationship, as it is being done for other tumours [21,22]. It is true that variations in radiosensitivity parameters (α, β) affect the TCP more [22] than variations in cellularity but, depending on the magnitude of inter-patients' variations, TCP_{ADC} contribution could still be relevant, showing a more conservative behaviour than TCP_{LIT}, as this study suggests.

In order to evaluate the robustness and the clinical applicability of the proposed method, a mathematical [22] or empirical [37], or hybrid, model of TCP variability based on robustly estimated data and a larger patients' pool should be implemented. Further analyses will focus on extending the proposed approach to alternative modelling strategies built upon a larger dataset.

Conclusions

In this work, a TCP model for skull-base chordoma patients treated with CIRT was enriched by including cellular density from DW-MRI. The inclusion of DW-MR information [22] seems to be a feasible path towards treatment personalization in particle therapy, showing more conservative tumour control predictions with respect to a model based on parameters from the literature. This could support clinical decision-making tools for treatment plans ranking or patients' risk stratification [38] when dose-escalation

studies are not available. However, further investigations on the ADC–cellularity relationship and the integration of normal tissue complication models in the current approach are required for a robust clinical usage.

Conflicts of interest

None.

Acknowledgement

The first author would like to thank Luca Anemoni for the initial support during data collection.

Appendix A. Supplementary data

Supplementary data to this article can be found online at https://doi.org/10.1016/j.radonc.2019.04.018.

References

[1] Durante M, Orecchia R, Loeffler JS. Charged-particle therapy in cancer: clinical uses and future perspectives. Nat Rev Clin Oncol 2017;14:483–95.
[2] Linz U, editor. Ion beam therapy. Berlin, Heidelberg: Springer Berlin Heidelberg; 2012.
[3] Suit H, DeLaney T, Goldberg S, et al. Proton vs carbon ion beams in the definitive radiation treatment of cancer patients. Radiother Oncol 2010;95:3–22.
[4] Walcott BP, Nahed BV, Mohyeldin A, et al. Chordoma: current concepts, management, and future directions. Lancet Oncol 2012;13:e69–76.
[5] Schardt D, Elsässer T, Schulz-Ertner D. Heavy-ion tumor therapy: physical and radiobiological benefits. Rev Mod Phys 2010;82:383–425.
[6] Schulz-Ertner D. Chordomas and chondrosarcomas: treatment with particle radiotherapy. In: Hayat MA, editor. Tumors of the central nervous system. Dordrecht: Springer, Netherlands; 2012. p. 173–83.
[7] Takahashi S, Kawase T, Yoshida K, et al. Skull base chordomas: efficacy of surgery followed by carbon ion radiotherapy. Acta Neurochir (Wien) 2009,;151:759–69.
[8] Schulz-Ertner D, Karger CP, Feuerhake A, et al. Effectiveness of carbon ion radiotherapy in the treatment of skull-base chordomas. Int J Radiat Oncol 2007;68:449–57.
[9] Owen JH, Komarck CM, Wang AC, et al. UM-Chor1: establishment and characterization of the first validated clival chordoma cell line. J Neurosurg 2018;128:701–9.
[10] Fujisawa H, Genik PC, Kitamura H, et al. Comparison of human chordoma cell-kill for 290 MeV/n carbon ions versus 70 MeV protons in vitro. Radiat Oncol 2013;8:91.
[11] Zou M-X, Lv G-H, Zhang Q-S, et al. Prognostic factors in skull base chordoma: a systematic literature review and meta-analysis. World Neurosurg 2018;109:307–27.
[12] Webb S, Nahum AE. A model for calculating tumour control probability in radiotherapy including the effects of inhomogeneous distributions of dose and clonogenic cell density. Phys Med Biol 1993;38:653–66.
[13] Stavreva N, Stavrev P, Warkentin B, et al. Derivation of the expressions for γ50 and D50 for different individual TCP and NTCP models. Phys Med Biol 2002;47:3591–604.
[14] El Naqa I, Pater P, Seuntjens J. Monte Carlo role in radiobiological modelling of radiotherapy outcomes. Phys Med Biol 2012;57.
[15] Karger CP, Peschke P. RBE and related modeling in carbon-ion therapy. Phys Med Biol 2017;63:01TR02.
[16] Mizoe J. Review of carbon ion radiotherapy for skull base tumors (especially chordomas). Reports Pract Oncol Radiother 2016;21:356–60.
[17] Tommasino F, Nahum A, Cella L. Increasing the power of tumour control and normal tissue complication probability modelling in radiotherapy: recent trends and current issues. Transl Cancer Res 2017;6:S807–21.
[18] Schmidt MA, Payne GS. Radiotherapy planning using MRI. Phys Med Biol 2015;60:R323–61.
[19] van der Heide UA, Houweling AC, Groenendaal G, et al. Functional MRI for radiotherapy dose painting. Magn Reson Imaging 2012;30:1216–23.
[20] Yeom KW, Lober RM, Mobley BC, et al. Diffusion-weighted MRI: distinction of skull base chordoma from chondrosarcoma. Am J Neuroradiol 2013;34:1056–61.
[21] Surov A, Hamerla G, Meyer HJ, et al. Whole lesion histogram analysis of meningiomas derived from ADC values. Correlation with several cellularity parameters, proliferation index KI 67, nucleic content, and membrane permeability. Magn Reson Imaging 2018;51:158–62.
[22] Casares-Magaz O, Van Der Heide UA, Rørvik J, et al. A tumour control probability model for radiotherapy of prostate cancer using magnetic resonance imaging-based apparent diffusion coefficient maps. Radiother Oncol 2016;119:111–6.
[23] Preda L, Stoppa D, Fiore MR, et al. MRI evaluation of sacral chordoma treated with carbon ion radiotherapy alone. Radiother Oncol 2018;128:203–8.
[24] Wolf MB, Edler C, Tichy D, et al. Diffusion-weighted MRI treatment monitoring of primary hypofractionated proton and carbon ion prostate cancer irradiation using raster scan technique. J Magn Reson Imaging 2017;46:850–60.
[25] Qi W-X, Zhang Q, Li P, et al. The predictive role of ADC values in prostate cancer patients treated with carbon-ion radiotherapy: initial clinical experience at Shanghai Proton and Heavy Ion Center (SPHIC). J Cancer Res Clin Oncol 2016;142:1361–7.
[26] Ginat DT, Mangla R, Yeaney G, et al. Diffusion-weighted imaging for differentiating benign from malignant skull lesions and correlation with cell density. Am J Roentgenol 2012;198:597–601.
[27] Bai J, Zhai Y, Wang S, et al. Prognostic value of a category based on electron microscopic features of clival chordomas. World Neurosurg 2017;99:282–7.
[28] Fowler JF. The linear-quadratic formula and progress in fractionated radiotherapy. Br J Radiol 1989;62:679–94.
[29] Wiklund K, Toma-Dasu I, Lind BK. Impact of dose and sensitivity heterogeneity on TCP. Comput Math Methods Med 2014;2014:1–7.
[30] Nahum AE, Tait DM. Maximizing local control by customized dose prescription for pelvic tumours. In: Breit A, Heuck A, Lukas P, editors. Tumor response monitoring and treatment planning. Springer, Berlin Heidelberg: Berlin, Heidelberg; 1992. p. 425–31.
[31] Newhauser W. International commission on radiation units and measurements report 78: prescribing, recording and reporting proton-beam therapy. Radiat Prot Dosimetry 2009;133:60–2.
[32] Mayles P, Nahum A, Rosenwald J-C. Biological evaluation of treatment plans. In: Handbook of radiotherapy physics: theory and practice. Boca-Raton: Taylor & Francis; 2007. p. 731–71.
[33] Friedrich T, Scholz U, Elsässer T, et al. Systematic analysis of RBE and related quantities using a database of cell survival experiments with ion beam irradiation. J Radiat Res 2013;54:494–514.
[34] Fossati P, Matsufuji N, Kamada T, et al. Radiobiological issues in prospective carbon ion therapy trials. Med Phys 2018;45:e1096–110.
[35] van Leeuwen CM, Oei AL, Crezee J, et al. The alfa and beta of tumours: a review of parameters of the linear-quadratic model, derived from clinical radiotherapy studies. Radiat Oncol 2018;13:96.
[36] Gulluoglu S, Turksoy O, Kuskucu A, et al. The molecular aspects of chordoma. Neurosurg Rev 2016;39:185–96.
[37] Deasy JO, Chao KSC, Markman J. Uncertainties in model-based outcome predictions for treatment planning. Int J Radiat Oncol 2001;51:1389–99.
[38] Walsh S, Roelofs E, Kuess P, et al. A validated tumor control probability model based on a meta-analysis of low, intermediate, and high-risk prostate cancer patients treated by photon, proton, or carbon-ion radiotherapy. Med Phys 2016;43:734–47.